CALIFORNIA INSTITUTE OF TECHNOLOGY

ELECTRON TUBE AND MICROWAVE LABORATORY

VACUUM TUBE RESEARCH PROJECT

QUARTERLY STATUS REPORT NO. 5

April 1, 1954 to June 30, 1954

A REPORT ON RESEARCH CONDUCTED UNDER

CONTRACT WITH THE OFFICE OF NAVAL RESEARCH

VACUUM TUBE RESEARCH PROJECT

CALIFORNIA INSTITUTE OF TECHNOLOGY

Pasadena, California

QUARTERLY STATUS REPORT NO. 5.

April 1, 1954 to June 30, 1954

Prepared under Contract Nonr 220(13)

Task Order No. 13

for

Office of Naval Research

Submitted by: Lester M. Field

QUARTERLY REPORT

Nonr 220(13)

Vacuum Tube Research Project

California Institute of Technology

This report covers the fifth three months of operation under this contract and is for the period April 1, 1954 through June 30, 1954.

The principal content of this report is a description of amplifying tube probe measurements, and their related analysis which have led to appreciable further understanding in our examination of the causes of saturation under attenuators and in drift spaces.

Further work in the examination of various proposed theories for the generation of radio noise is described.

The beginnings of further work in M-carcinotrons is discussed.

Finally, the beginnings of our effort to apply ferrites to slow-wave propagating structures is described.

Project A - Theoretical Studies of the True Tape Helix and Application to Electrostatically Focused Bifilar Backward-Wave Oscillators

This work was not active during the period reported here, but will be reactivated during the following quarter with the completion of a new tube for these purposes.

Project B - Backward Wave Oscillator Efficiency

This work is closely related to that of Project A and was not active during this period but will be reactivated in connection with Project A.

Project C - Power Limitation in Forward Gain Amplifier Tubes by Attenuator Saturation

Staff: T. E. Feuchtwang, W. Buchman, E. V. Nogle, L. M. Field

Concurrent with our theoretical investigations, a number of experiments were conducted.

A. Procedure: To permit ready observation of saturation effects, a low power traveling-wave tube was constructed. The average operating conditions at 3000 mc are indicated below:

C	Q	QC	N	V Helix	I Beam	Driver
.038	3.18	.12	59	650 V	.9 m A	2K 41 Klystron

The experimental set up is sketched below:

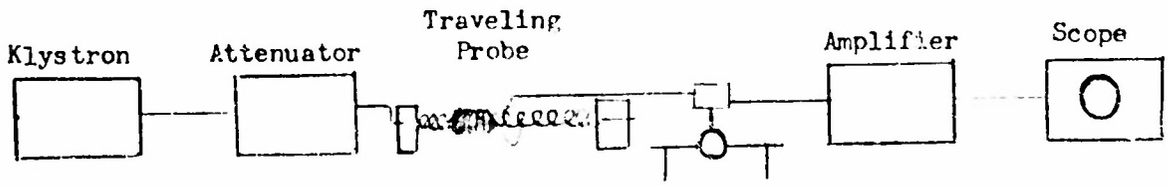

Figure 1.

The r.f. probe consisting of a single turn coupled helix slid along the outside of the tube. The probe-Xtal-amp-scope combination was calibrated by cold measurements to give a conversion of scope units to power on the helix in dbm.

B. Discussion of Results: With this set up, several runs of power (on the helix) vs. distance (along the helix) were carried out. The parameters used were (1) attenuator length

(2) driving power.

2" attenuator: On Figure 2, a number of plots of power vs. distance are displayed. The data was taken with a 2" attenuator placed about 2" beyond the helix beginning. We clearly observe three distinct regions.

(1) The exponential rise before the center attenuator (transformed by use of log scale into a straight line)

(2) The irregular field picked up over the attenuator

(3) The rise beyond the attenuator.

It is noticeable that increased drive results in (i) reduction of the gain/unit length, (ii) decrease of the length of the output section in which gain occurs, and (iii) failure of the gaining wave to build up altogether. The sequence corresponds in our previous terminology to, (i) possible partial saturation of the beam because of hash which reduces the size of the active beam and possibly the introduction of a velocity scatter which diminishes gain; (ii) hash level much higher than useful signal, beam quite saturated, and possibly only after the lower order plasma waves have gone through sufficient phase change to cause a partial cancellation of velocity scatter does enough gain per length occur to permit the signal to start rising again; (iii) beam completely saturated by hash (a.c. hash current density peaks exceed d.c. current density).

Calculations of the a.c. current hash and a.c. velocity scatter pertinent to the tube tested here are described in a later section of this report. From such calculations, whose essence as far as current hash is concerned is summarized in Figure 6, one can attempt to predict the level at which saturation sets in using various lengths of attenuators. In curves of the type shown in Figure 2 and Figure 3 the differences between short and long attenuators are difficult to discern. Inasmuch as only a gross saturation effect at an appreciable distance beyond the end of the

attenuator is clearly evident and as we can see from the theoretical work as exemplified in Figure 6, at an appreciable distance beyond the end of the attenuator saturation levels are pretty much the same for a variety of attenuator lengths, it is evident that we can expect little difference between short and long attenuators observed on this basis. (It should be noted we consider that insofar as the saturation caused by high order modes is concerned, that the high order modes continue to build up in the same way in the output helix section beyond the attenuator that they would under an attenuator. At least this is the simple postulate we make subject to later slight modification by more advanced analysis. The measurements shown on Figure 5 seem to lend experimental support to this idea.)

In order to test the predictions of Figure 6 much more closely than is possible with the type of measurements made on Figure 2 and Figure 3, a specific test of saturation levels at various distances beyond the end of the attenuator was made and will be described later in this report.

There are, however, some fine scale features of the measurements made and described in Figures 2 and 3 which it may be possible to examine on theoretical grounds. In Figure 2, for example, at a certain drive level the amplification after the attenuator continues but has been markedly reduced. We are currently attempting to theoretically predict the magnitude of this effect and this work will be reported on in our next quarterly report. We also observed on Figure 2 that at a somewhat higher drive level amplification cannot start in the helix after the attenuator until we have traversed about 10 cm, at which point the gain again comes into being. We shall try to predict this effect on the basis of our theoretical current and velocity distribution curves and discuss it in our next report.

In connection with the curves just discussed, the significance

Power on the Helix vs. Distance along the Tube for a 2" Attenuator

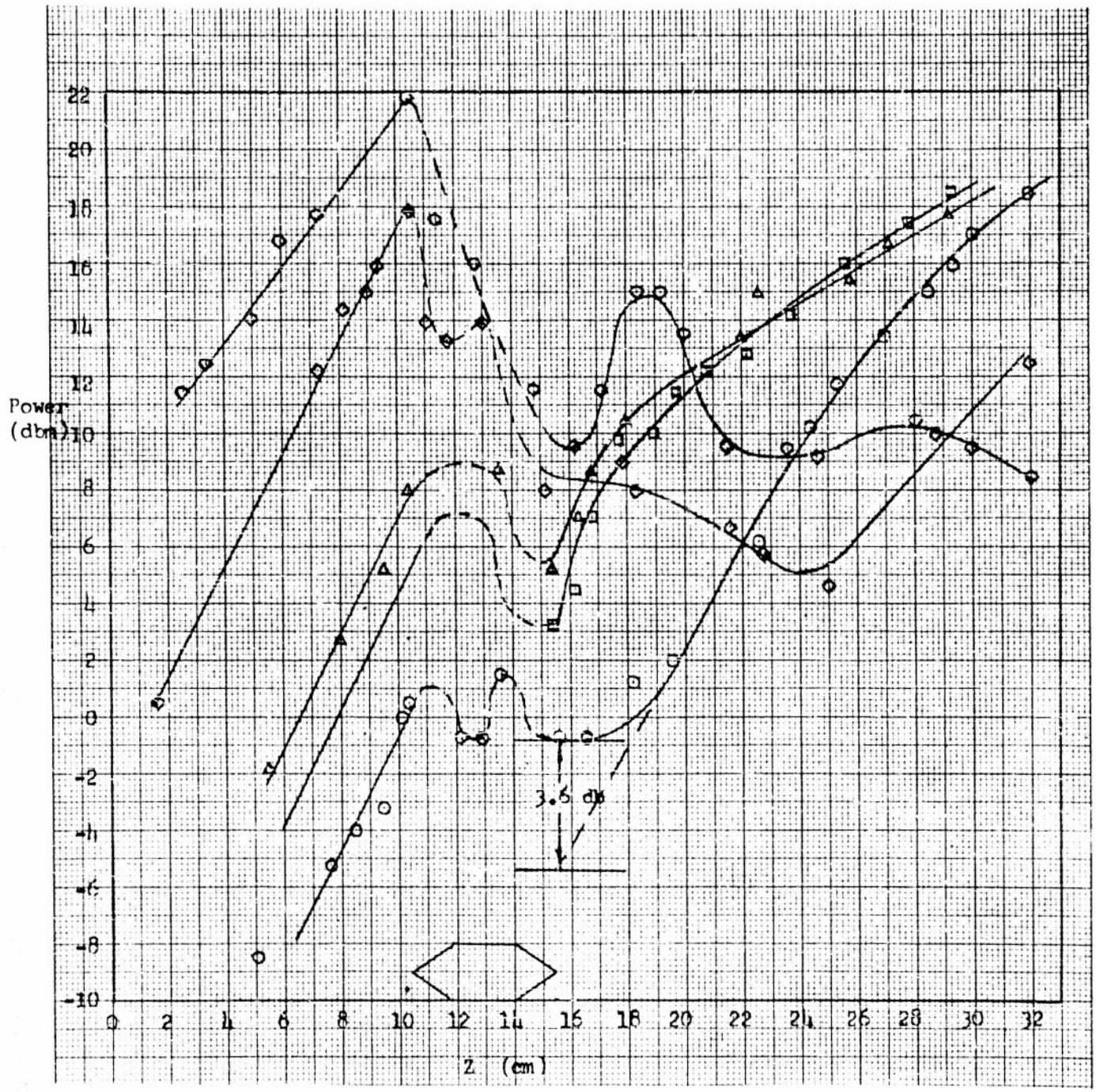

Figure 2.

Power on the Helix vs. Distance along the Tube for a

5" Attenuator

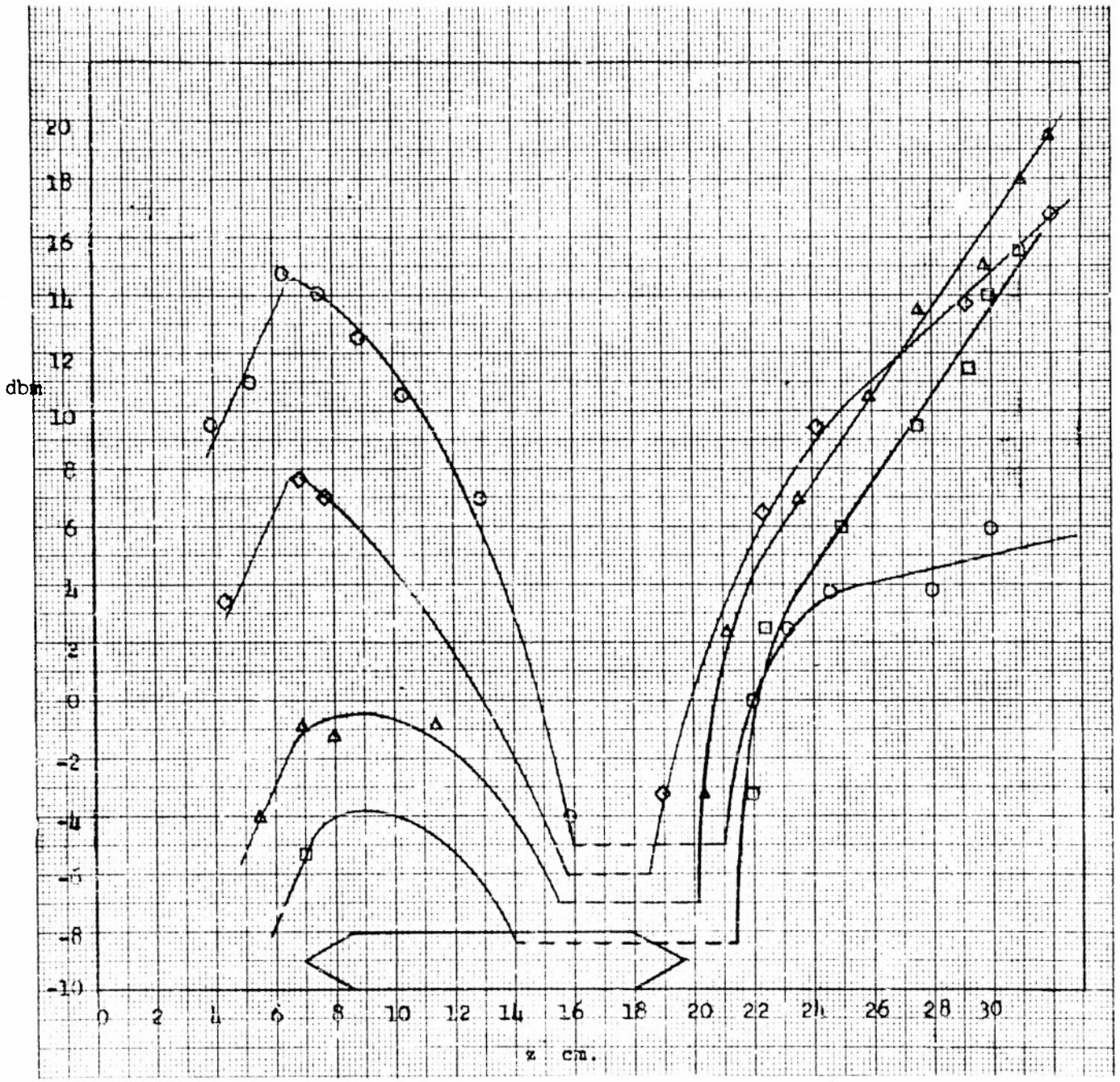

Figure 3.

of the readings over the attenuator was questioned. Since the probe was coupled to the helix only, that is, detected only energy actually traveling on the helix, it seems that the assumption that the helix and attenuator combination acted like a drift space was not quite satisfied, and that the helix probably propagated some energy. If, as the case seems to be, this energy was propagating in a high velocity mode, the coupling to the probe was much increased over that of the slow waves. Consequently whatever energy was detected was at a proportionately much lower level, i.e., the plot is probably quite misleading in the attenuator region. It is moreover possible that some admittance wall amplification does occur in the attenuator. Both these possibilities will be further investigated in the future. A second point of interest is the fact that the output signal does not start from zero ($-\infty$ on the log scale). This may be explained as follows: Because of the taper in the attenuator, the regular gain process starts somewhere before the end of the attenuator. At the same time the propagation of the fast mode on the outside of the attenuator is reduced. These two effects tend to add in such a way as to wash out the transition from attenuator to helix. It is interesting to note that at low drive levels, the extrapolated signal at the output of the attenuator is about 4 db below the input to the attenuator.* This result checks with the calculations.

5" attenuator - Figure 3 shows a set of power vs. distance curves like those in Figure 2, but taken with a 5" attenuator. The general tendency is unchanged, however, the drive level producing saturation is somewhat lower. The transition from attenuator to helix is quite pronounced in this

---

* This equivalent signal was obtained by extrapolating the final field vs. distance plot back to the attenuator output (see Fig. 2).

case. Apparently, the transmission of the fast mode (see above) dropped considerably before the end of the attenuator was reached, so that when the exponential growth could start again, no other energy was traveling on the helix. There was not enough length of helix beyond the attenuator to observe saturation due to the tube itself. The fact that the amount of damage done by the attenuator is a function of its length is difficult to observe with respect to Figures 2 and 3 as previously discussed. In order to check this point quite carefully, the experiment described next was carried out.

Relative Drive Required to Give Absolute Saturation vs. Distance beyond Attenuator: To supplement the curves discussed above, a different set of measurements was taken. Taking as a criterion the relative drive at the input of the attenuator necessary to produce a maximum field along the helix beyond the attenuator, measurements of drive producing saturation vs. distance beyond attenuator were taken. The saturation defined above is much more severe than that usually considered, i.e., not only is there a drop in gain with increased drive, but the actual field at the point in question drops with increased drive. The relative drive was determined by the setting of the input attenuator. In order to preserve identical input conditions, the attenuator length was changed by removing parts of the output end of the attenuator, leaving the input end unchanged.

The curves seem to indicate that the amount of damage done by center attenuators of different lengths approaches an upper bound. (Figure 4). The curves were replotted with distance measured from a fixed point along the tube (Figure 5). Calculations have checked fairly well the difference between the first points of each of the three curves on Figure 4. This was done by calculating a theoretical curve giving relative drive

Relative Power Level to Saturate
vs.
Distance from End of Attenuator

(experimental)

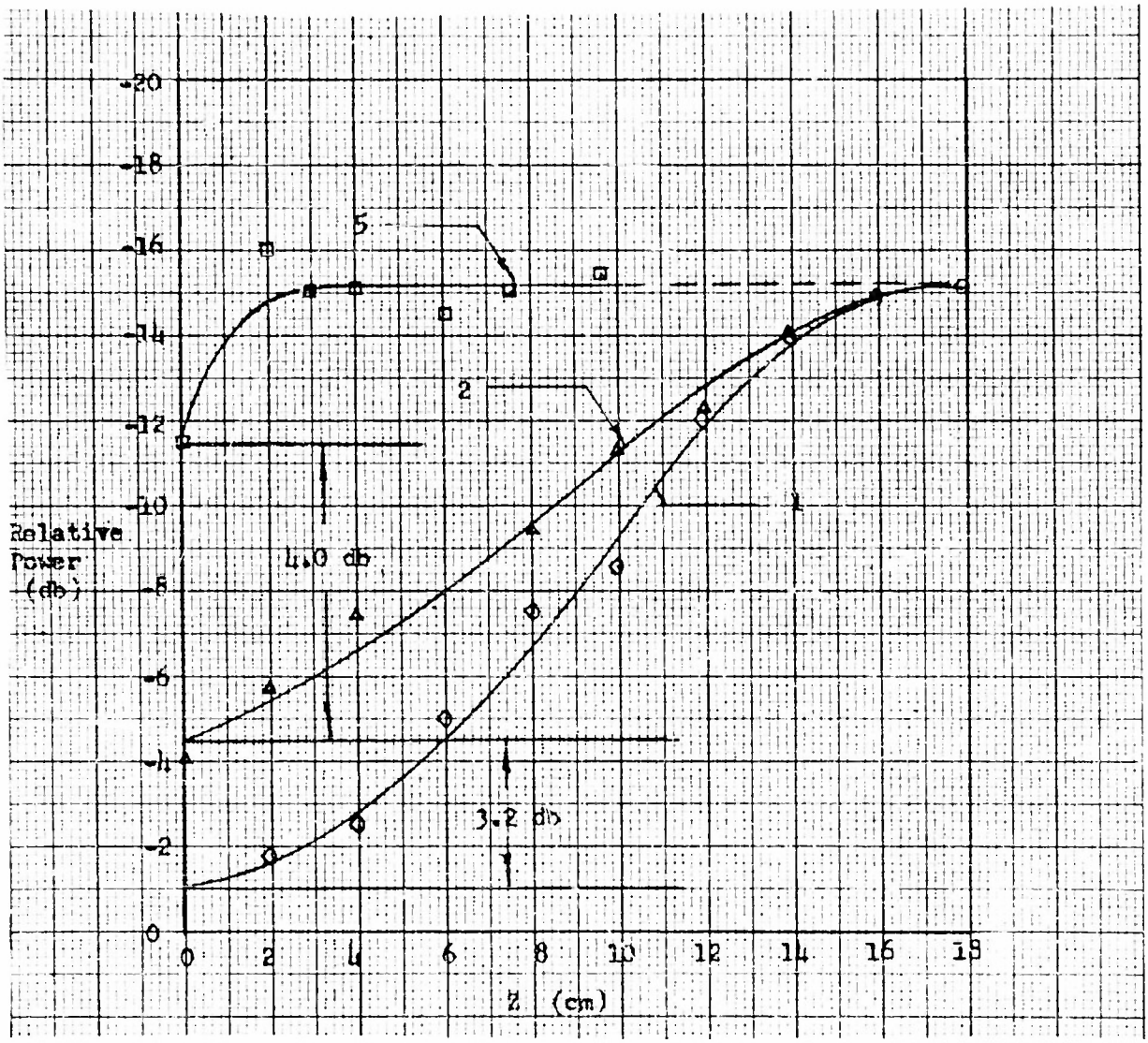

Figure 4.

Relative Power Level to Saturate

vs.

Distance along the Tube

(experimental)

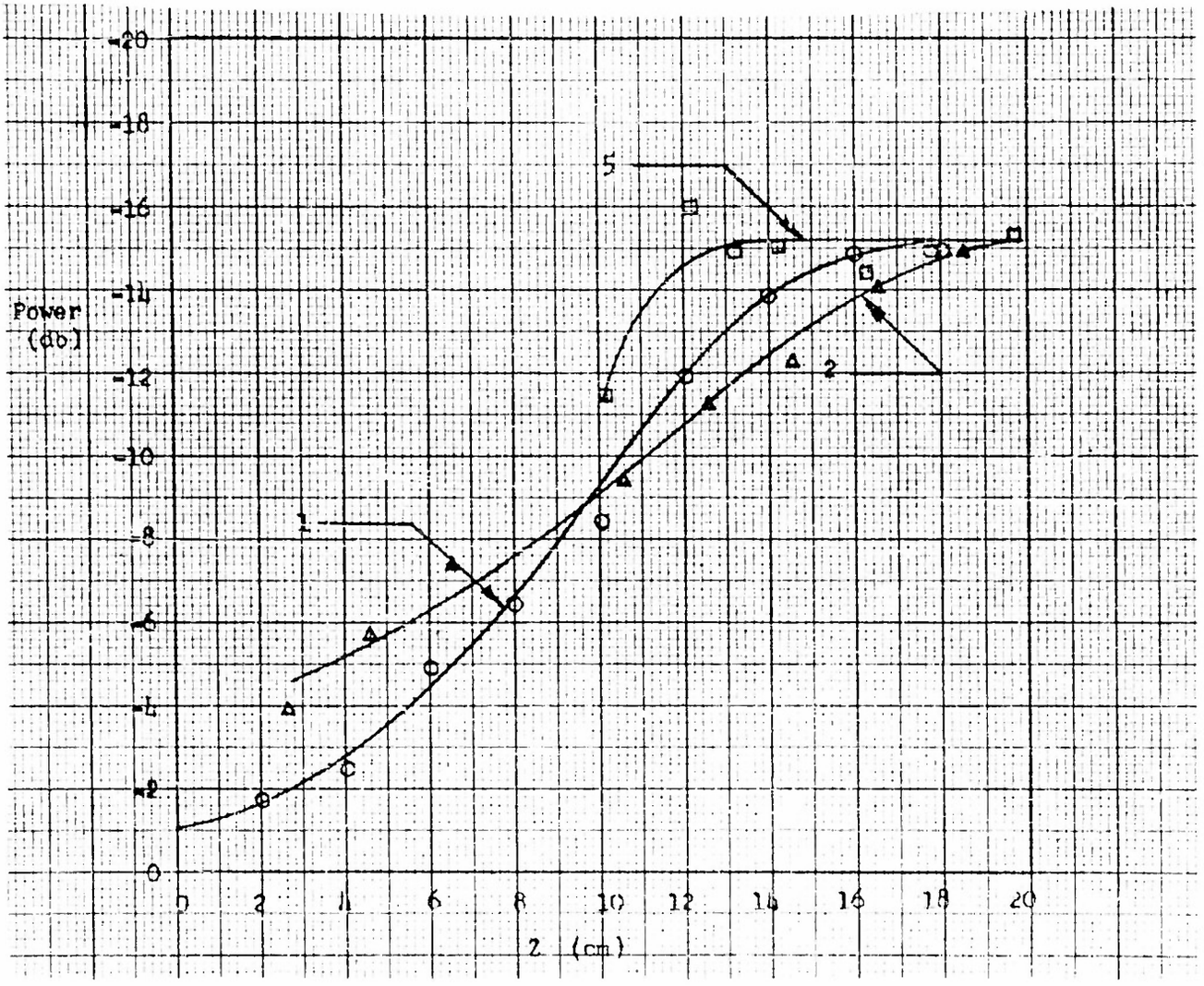

Figure 5.

Ratio of Peak Current Density at End of Attenuator
to Peak Current Density at Beginning of Attenuator
vs.
Length of Attenuator

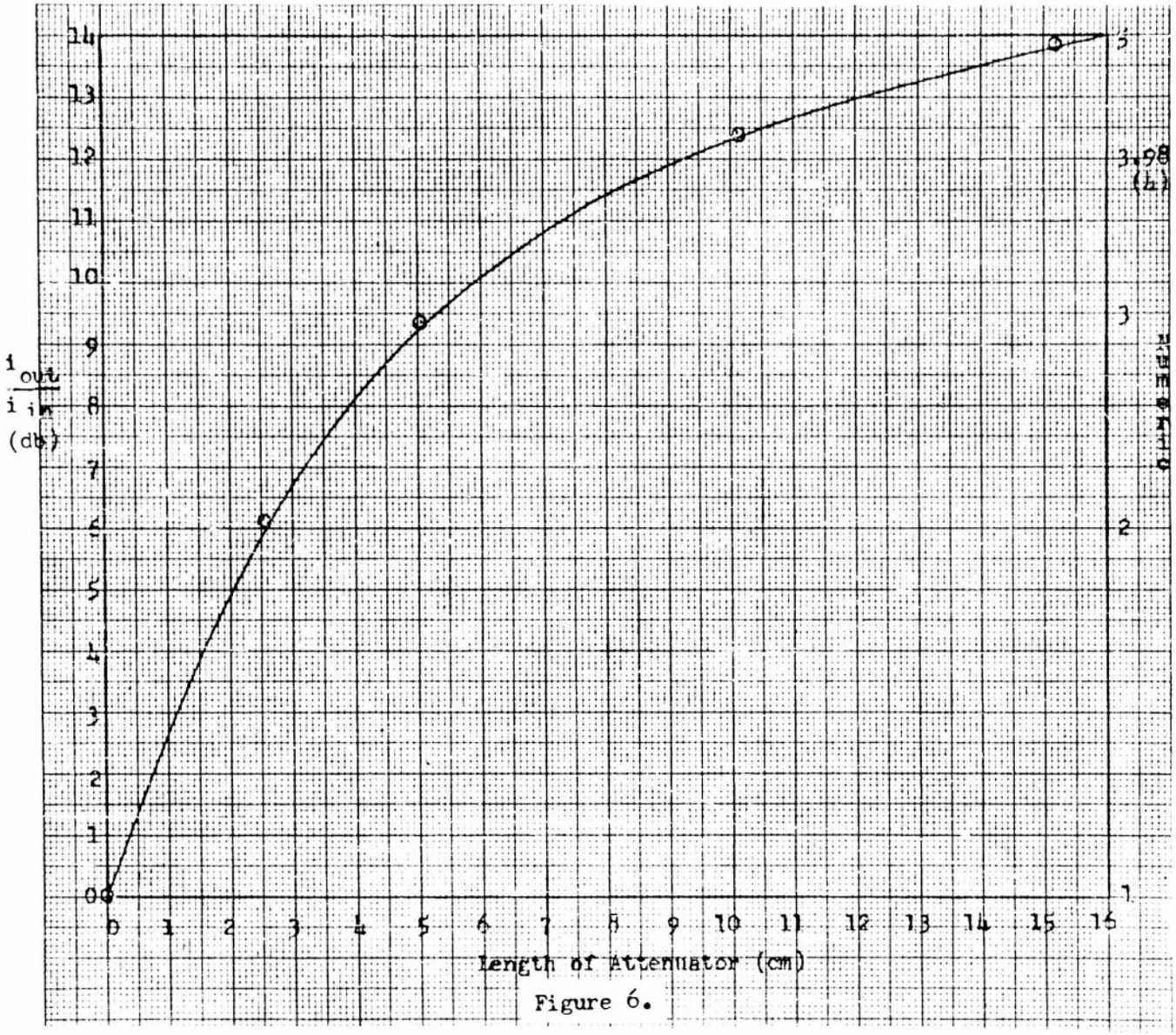

Figure 6.

$$\frac{i_{out}}{i_{in}} = \frac{2\, I_o(\beta_e a) \sum_{o}^{7.5} RM\, J_o(0.9\ \tau_n a)}{I_o(\beta_e a)}$$

$$R = \frac{\tau_n a}{(\tau_n a^2 + \beta_e a^2)\, J_1(\tau_n a)}$$

$$M = \cos \frac{\beta_\rho z}{\sqrt{1 + \left(\frac{\tau_n a}{\beta_e a}\right)^2}} + j\, e^{j\frac{4}{3}\pi} \sqrt{1 + \left(\frac{\tau_n a}{\beta_e a}\right)^2}\ C \frac{\beta_e}{\beta_\rho} \sin \frac{\beta_\rho z}{\sqrt{1 + \left(\frac{\tau_n a}{\beta_\rho a}\right)^2}}$$

producing saturation at the end of the attenuator, vs. attenuator length. (Figure 6. In computing this curve saturation was considered to set in when $i_{ac} = i_{dc}$ using the high order mode summation plot of Figure 7.) We are currently using the information plotted in the remaining figures of this section to attempt to predict the variation in saturation level vs. distance from the end of the attenuator which was measured in Figure 4. In addition, as previously remarked, we are attempting to use our velocity distribution curves to predict changes in gain beyond the attenuator and the ability of the tube to resume gain after having transversed an appreciable length beyond the attenuator without showing evidences of gain. Such calculations will be described in our next report.

APPENDIX TO PROJECT C

A.C. Current and Velocity Profiles: As a byproduct of the calculations mentioned above, the radial distributions of a.c. current densities (i) and a.c. velocities (v) were obtained for various lengths of attenuators. The calculations do not take into account the fact that the beam does not completely fill the inside of the helix. Some representative plots and calculations are given below.

It is interesting to note that the calculations indicate:

(1) As the length of the attenuator increases, the currents and the velocities at different radii show considerable phase differences. To account for this instantaneous profiles were also drawn with the time reference chosen when the greatest a.c. peak went through its absolute maximum.

(2) The current density peak is always very close to the edge of the beam, while the velocity peaks occur at radius which varies markedly from section to section.

Figure 7

ABSOLUTE MAGNITUDE OF CURRENT DENSITY AT DIFFERENT RADII

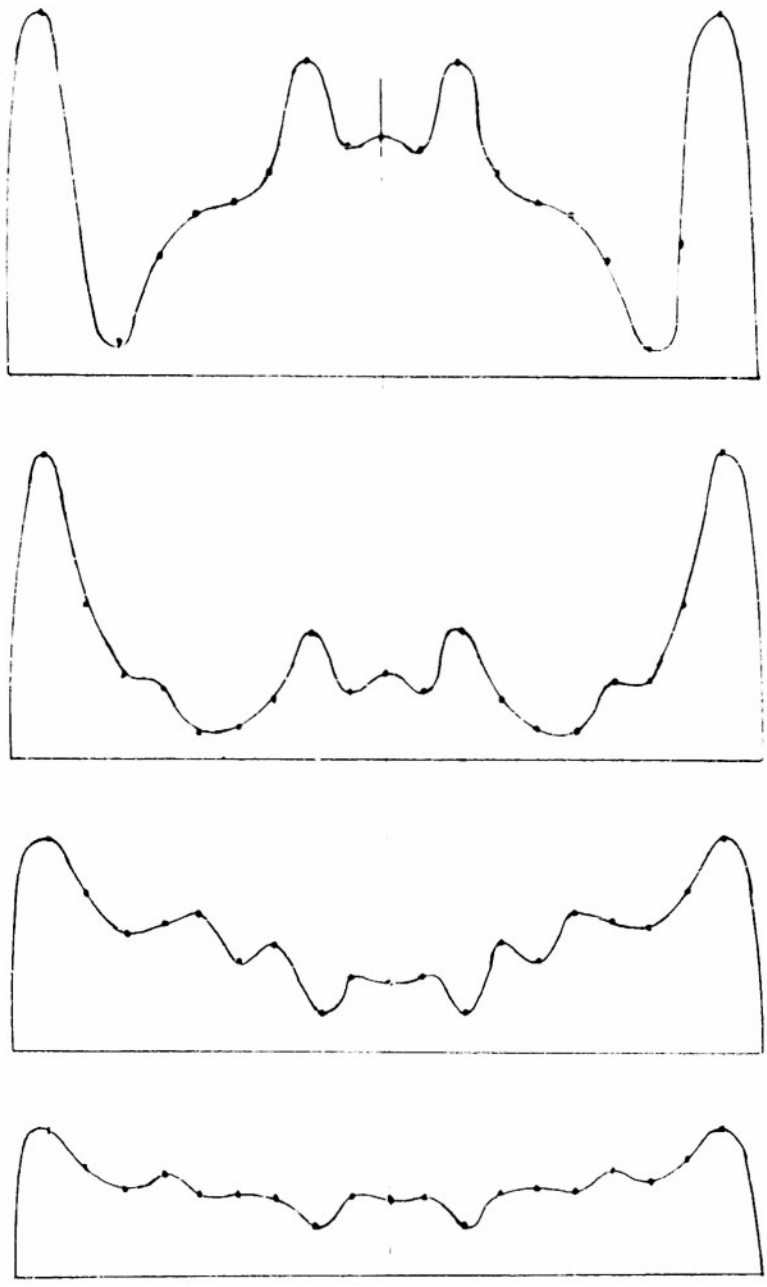

15.24 cm attenuator

10.16 cm attenuator

5.08 cm attenuator

2.54 cm attenuator

• computed point

Figure 8
INSTANTANEOUS CURRENT DENSITY PROFILES TAKEN AT INSTANT OF MAXIMUM AMPLITUDE OF GREATEST CURRENT DENSITY PEAK

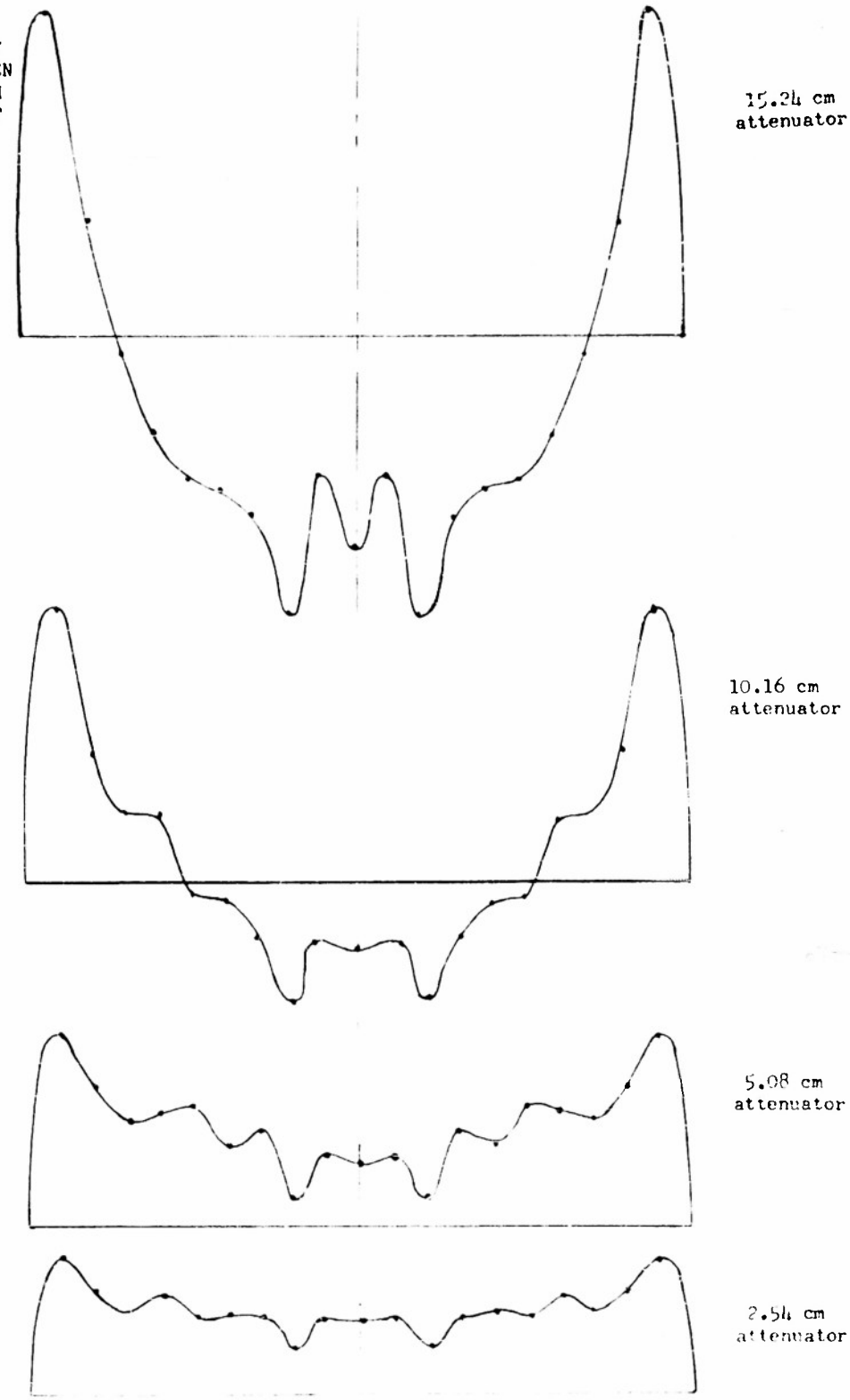

• computed point

Figure 9
ABSOLUTE MAGNITUDE OF VELOCITIES AT DIFFERENT RADII

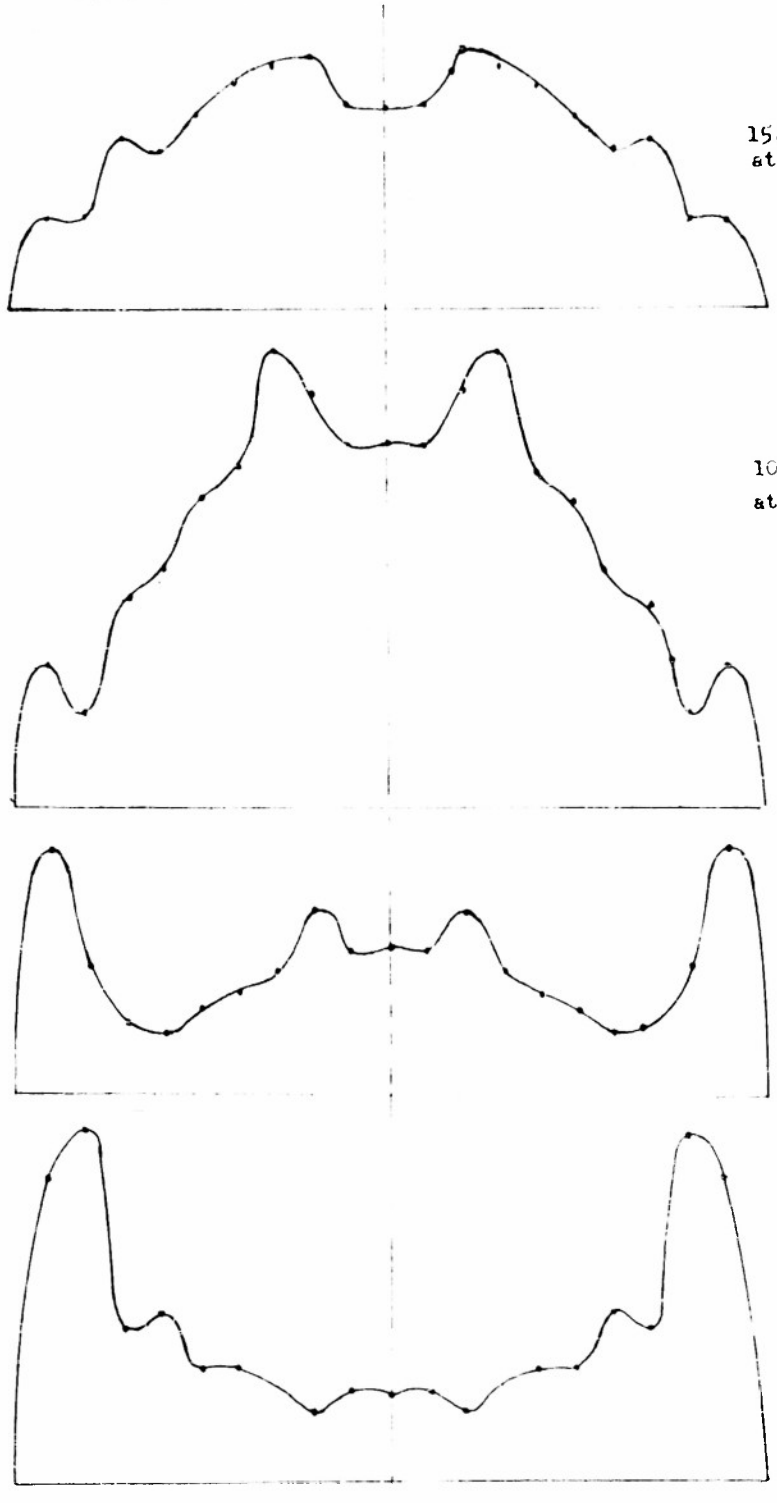

Figure 10
INSTANTANEOUS VELOCITY PROFILES TAKEN AT INSTANT OF MAXIMUM AMPLITUDE OF GREATEST VELOCITY PEAK

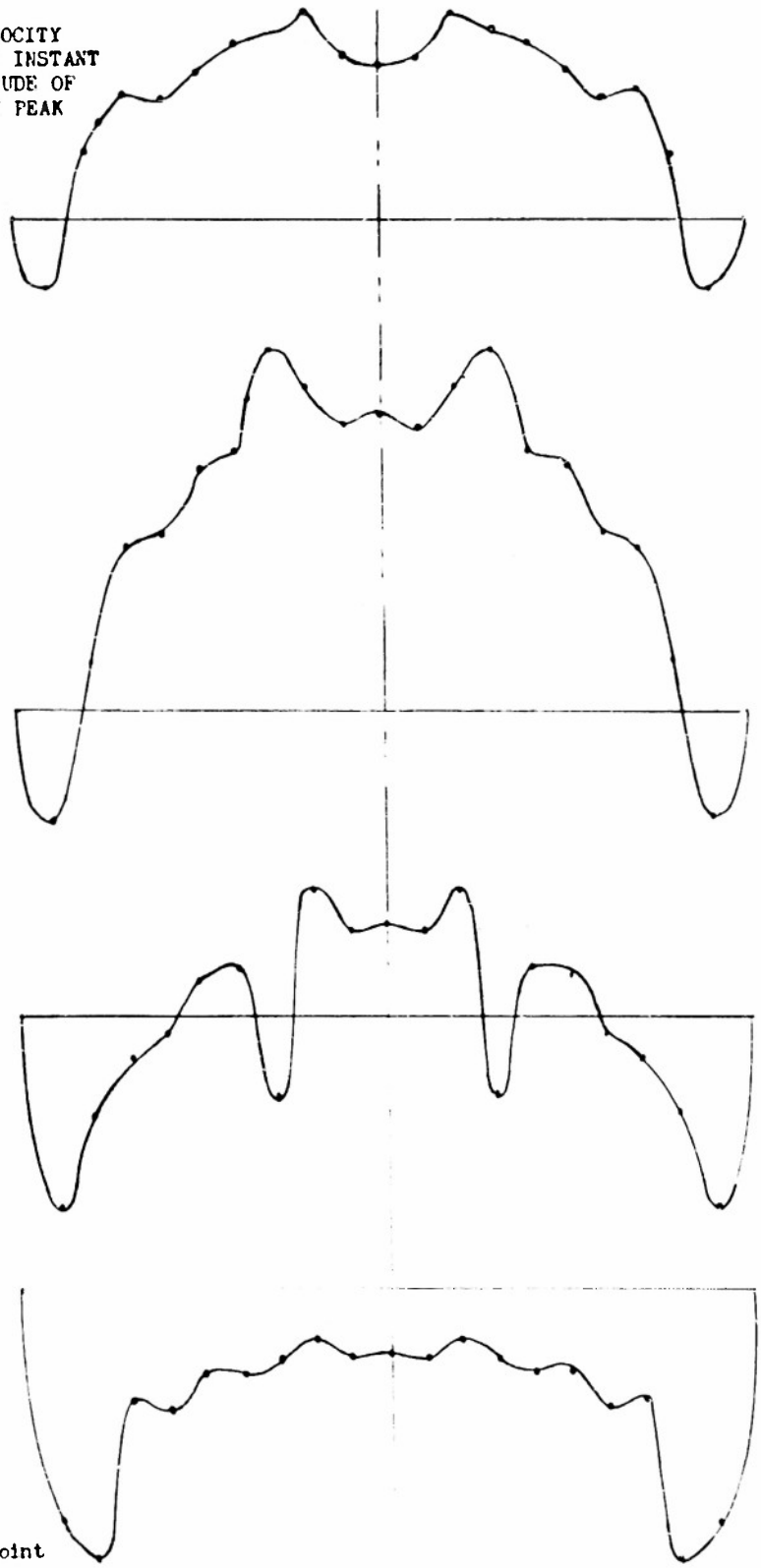

• computed point

TABULATION OF RESULTS

$\frac{i}{2\, i_o\, I_o(\beta_e a)}$ at the end of the attenuating section vs. length of attenuator (in cm.)

z \ r/a	0	.2	.4	.6	.8	.9
2.54	.538 | -17.05°	.364 | -17.4°	.608 | -16.7°	.7159 | -20.79°	.767 | -16.7°	1.013 | -15.6°
5.08	.487 | -28.5°	.252 | -43.7°	.618 | -26.0°	.885 | -23.7°	1.08 | -22.1°	1.46 | -21.1°
10.16	.524 | 176.3°	.898 | 167.4°	.230 | -153.6°	.514 | -42.1°	1.05 | -10.4°	2.09 | -26.0°
15.24	1.633 | 159.1°	2.14 | 158.2°	1.167 | 161.2°	.793 | 171.9°	.875 | -33.4°	2.465 | -27.8°

$$\frac{\left|\frac{i}{i_o}\right| \text{ peak out of attenuator}}{\left|\frac{i}{i_o}\right| \text{ peak into attenuator}} \quad \text{vs. Attenuator Length}$$

Z cm	$\frac{(i/i_o) \text{ peak out}}{(i/i_o) \text{ peak in}}$	$\frac{(i/i_o) \text{ peak out}}{(i/i_o) \text{ peak in}}$ in db
0	1	0
2.54	2.026	6.12
5.08	2.92	9.32
10.16	4.18	12.44
15.24	4.93	13.88

Velocity Profiles,

Values plotted are $\frac{v \times 10^2}{2 v_o I_o (\beta_e a)} = \frac{v \times 10^2}{2 \frac{i_o}{\rho_o} I_o (\beta_e a)}$ at the End of an Attenuator vs.

Attenuator Length (in cm.)

z \ r/a	0	.2	.4	.6	.8	.9
2.54	-.455 | 24.2°	-.355 | -1.2°	.594 | 36.8°	-.901 | 47.9°	1.883 | 29.8°	-1.635 | 36.3°
5.08	-.800 | -87.4°	1.01 | 84.3°	-.548 | -75.1°	-.335 | -10.8°	.694 | 43.3°	-1.34 | 55.2°
10.16	2.05 | 67.1°	2.27 | 66.3°	1.795 | 68.7°	1.235 | 72.7°	-.358 | -89.4°	-.798 | 51.8°
15.24	1.10 | 57.8°	1.425 | 49.3°	1.225 | 45.5°	.865 | 62.0°	.487 | 60.4°	-.488 | 60.8°

Amplitude of the I_o^{th} Component of a.c. Current Density and a.c. Velocity at the Output of an Attenuator, vs. Attenuator Length (in cm.)

z	A_i	A_v
2.54	1.745	-.02640
5.08	2.130	-.01008
10.16	1.789	.01695
15.24	.830	.01179

$i = 2 i_o I_o (\beta_e a) A_i I_o (\beta_e r)$; $v = 2(i_o/\rho_o) I_o (\beta_e a) A_v I_o (\beta_e r)$

SAMPLE CALCULATIONS

(1) Design Parameters.

V_o = 650 volts

I_o = .5 mA

2b = 1.27 mm = beam diameter

2a = 2.31 mm = mean helix diameter

$$u_o = \frac{c\sqrt{V_o}}{505} = \frac{c}{22.6}$$

$\beta = 19.4\,\beta_o$

g = .518 cm (at 3000 mc)

$\frac{2\pi a}{\lambda g} = \gamma_o a = 1.40$

$K_e = (15)(19.4)$ (Read from Chart A6.5, p.250, Pierce)

Correction for actual helix $\frac{K_a}{K_e} = .55$ (Cutler Chart)

C = .034

Q_e = 1.75 (A 6.4, p.249 Pierce)

Q_a = 1.75/.55 = 3.18

QC = .11

Note: These calculations were based upon the design data and were started before the actual experimental runs, hence the slight discrepancy between the assumed and actual values of I_o and V_o. However, the difference is smaller than the probable error in the experimental data.

(2) Current and velocity profiles at the output of various lengths of attenuator:

Equations used:

$$i = 2i_o I_o(\beta_e a)\, e^{-j\beta_e z} \sum_{n=1}^{\infty} \frac{\tau_n a}{(\tau_n a)^2 + (\beta_e a)^2} \frac{J_o(\tau_n r)}{J_o(\tau_n a)}$$

$$\left\{ \cos \frac{\beta_p z}{\sqrt{1 + \left(\frac{\tau_n a}{\beta_e a}\right)^2}} + je^{j\frac{4\pi}{3}} \sqrt{1 + \left(\frac{\tau_n a}{\beta_e a}\right)^2}\; C \frac{\beta_e}{\beta_p} \sin \frac{\beta_p z}{\sqrt{1 + \left(\frac{\tau_n a}{\beta_e a}\right)^2}} \right\}$$

$$v = 2 I_o(\beta_e a) \frac{i_o}{\rho_o} e^{-j\beta_e z} \sum_{n=1}^{\infty} \frac{\tau_n a}{(\tau_n a)^2 + (\beta_e a)^2} \frac{J_o(\tau_n r)}{J_1(\tau_n a)}$$

$$\left\{ Ce^{j\frac{4\pi}{3}} \cos \frac{\beta_p z}{\sqrt{1 + \left(\frac{\tau_n a}{\beta_e a}\right)^2}} + j\frac{\beta_p}{\beta_e} \frac{1}{\sqrt{1 + \left(\frac{\tau_n a}{\beta_e a}\right)^2}} \sin \frac{\beta_p z}{\sqrt{1 + \left(\frac{\tau_n a}{\beta_e a}\right)^2}} \right\}$$

where $\tau_n a$ = nth zero of J_o

i_o = current density on axis of tube at the entrance of the drift space

$\beta_p = \frac{1}{u_o} \sqrt{\frac{\eta I_o}{\varepsilon_o u_o \pi b^2}} = 46.0\ m^{-1}$

$\beta_e = 1218\ m^{-1}$

u_o, I_o are d.c. velocity and d.c. total beam current respectively

$\eta = \frac{e}{m} = \frac{\text{electron charge}}{\text{electron mass}}$

(3) Extraction of the I_o^{th} component of a.c. velocity and a.c. current at the output of an attenuator.

As discussed in progress reports No. 2 and No. 3, the modes encountered in our analysis are not orthogonal. We are assuming for the moment, however, that the error introduced by assuming them to be orthogonal is not

large. As a first approximation we therefore considered I_o (the useful signal) and the modes generated in the attenuator to be orthogonal and extracted the I_o component of the current and velocity entering the helix from the attenuator, by evaluating graphically

$$\frac{\int_o^a r\ I_o(\beta_e r)\ \frac{i}{2i_o}\ I_o(\beta_e a)}{\int_o^a r\ I_o^2(\beta_e r)} = A_i$$

and setting $\frac{i}{2i_o\ I_o(\beta_e a)} = A_i\ I_o(\beta_e r)$

and similarly $\frac{v}{\frac{2i_o}{\rho_o}\ I_o(\beta_e a)} = A_v\ I_o(\beta_e r)$.

In the method which is now being worked on and which will be described in the following section of this report the true modes--both gaining and high order--come out automatically, but one is still faced with the problem of determining the proper relative amplitudes in view of their not being orthogonal.

Project D - Proposed Method of Expansion of Traveling-Wave Tube Fields into Modes

Staff: W. Buchman, L. M. Field

In addition to the study of appropriate methods for determining the relative amplitudes of the non-orthogonal modes existing under an attenuator or in a helix when excited by an arbitrary radially varying current, extensive computations have begun on the following problem. We propose to compute the solutions for a limited number of cases of the complete field theory

of a beam propagating under a helical conducting sheet which has near it a surrounding resistive sheet serving as an attenuator. In the case of the helix alone following the attenuator, the analysis will also apply, but the resistive sheet will be absent. The method is essentially as follows. We use as a basis the impedance wall amplifier charts of Birdsall and Whinnery except that we will extend these to include several higher order modes by computation. Given a certain size beam, frequency, velocity of electrons and charge density, these charts will give the propagation constants indicating gain or decay and phase, of all modes which can be excited in the stream including both the main gaining wave--principally of I_o form--and the higher order waves--principally of J_o form--provided that one knows the complex impedance at the surface of the beam which produced by the surroundings. Actually, of course, with a lossy propagating medium surrounding the beam the I_o and J_o form just mentioned will have complex arguments and hence not be a pure I_o or J_o variation.

In order to solve the problem it is required that next we make charts of the impedance presented to the beam by the external circuit. To our knowledge this has not been done in any appreciable generality or complexity and we propose to do it for a sheath helix with a resistive sheet surrounding the sheath helix. We are plotting the impedance at some radius inside of the sheath helix corresponding to the beam radius, as a function of complex propagation constant. Then by superimposing plots taken from the Birdsall and Whinnery work and these new plots from our own computations, one can find where the same complex impedance in both plots exists with the same complex propagation constant. This will occur at a number of points and each one of these points corresponds to one of the modes of the complete solution. These computations are now being prepared for the digital computer.

Inasmuch as our attenuator saturation studies have shown that in many practical tubes gain effects occur under the attenuator and these may be pure resistance wall or may be associated with propagation, we believe a solution of the complete problem at least for a few special cases will shed much new light on the subject.

Project E - A Study of the Relation between Microwave Noise Generation Processes and Possible Noise Generation Processes in Radio Astronomy.

Staff: R. W. Gould, L. M. Field

Outline of subjects worked on:

I. Non-linear Theory of Plasma Oscillations - An exact solution to the equations describing a beam of monoenergetic electrons has been obtained for the case where the disturbance is in the form of a traveling wave,

$$\bar{\Phi} = \frac{2e\phi}{m} = \bar{\Phi}(x - Vt) \quad .$$

It is

$$\frac{\omega_p x}{V} = -\sqrt{-(2+\bar{\Phi}) + 2\sqrt{1+\bar{\Phi}} + 2\varepsilon} \quad -\sin^{-1} \quad \frac{1-\sqrt{1+\bar{\Phi}}}{\sqrt{2\varepsilon}}$$

where ϕ = electrostatic potential

V = wave velocity

ω_p = plasma frequency of the stream

ε = amplitude parameter, which $\rightarrow 0$ for small amplitudes.

The small amplitude approximation is $\Phi = 2\sqrt{2}\,\epsilon \sin \frac{\omega_p x}{V}$ and the period of the exact solution is independent of amplitude. The form of the exact solution is not convenient for calculation of any of the quantities which might be of interest, e.g., frequency spectrum and energy density, but it should be possible to calculate the energy density for small signals correct

to second order without difficulty.

II. A. C. Energy in an Electron Stream - A conservation theorem for a.c. energy has been derived under the assumptions that the linearized equations of motions are the rigorously correct ones, that the velocities are non-relativistic, magnetic forces neglected, and that the d.c. flow of the stream is uniform. Such a theorem allows one to work completely within the linear theory when computing quadratic quantities such as kinetic and potential energies, provided one takes as definitions of these quantities, the quantities which appear in a natural manner in the conservation theorem. The theorem may be written,

$$\frac{\partial}{\partial t}\left[\frac{m}{e}\left(\frac{\rho_o v^2}{2} + \rho\, u_o \cdot v + \frac{\varepsilon E^2}{2}\right)\right] + \nabla \cdot \left[(u_o \cdot v)i\right] = 0$$

where quantities without subscripts are a.c. quantities and quantities with the subscript zero are the d.c. or steady quantities. One may then interpret the result as follows:

$\frac{\rho_o v^2}{2} + \rho\, u_o \cdot v$ = kinetic energy density

$\frac{\varepsilon E^2}{2}$ = electric field energy density

$(u_o \cdot v)i$ = vector power flow

This seems to be in general agreement with definitions proposed by others, although there is still some confusion, and in particular, the definition of kinetic energy density is at variance with that suggested by Heffner[1] and the definition of power flow, although conforming to usage of others, is at variance with the result of Tonks who used the correct non-linear equations of motion.

III. Double Stream Amplification. - The process of double stream amplification is being considered in considerable detail because it seems to be the most likely explanation of the large amounts of noise from solar flares. The simplest model which contains at least some of the essential features, including amplification, was first analyzed by Pierce[2] in connection with another problem and consists of a stream of charged particles moving with average velocity in through another system of charged particles with zero average velocity. The result of this analysis is that for plane disturbances of the form $e^{j(\omega t - \beta \cdot x)}$, β is given by,

$$\beta u_1 = \omega \pm \frac{\omega_1}{\sqrt{1 - \frac{\omega_2^2}{\omega^2}}} \qquad (a)$$

where ω_1 is the plasma frequency of the moving stream and ω_2 is the plasma frequency of the stationary stream.

Of particular interest is the circumstance under which solutions which represent increasing waves may be excited and the method suggested by Twiss[3] has been applied. This consists of finding the transient solution and requiring that, at a point x, there be no disturbance before $t = x/u_o$. In some cases this procedure rules out certain solutions, e.g., the incoming waves of the ordinary wave equation, but the result of this analysis was to show that both the increasing and decreasing waves are excited by an arbitrary disturbance at $x = 0$ whose frequency is less than the plasma frequency of the stationary stream.

In order to gain further understanding of the steady state growing wave solution, an energy balance was prepared using the definitions given in II. The time average kinetic energy of the stationary stream was found to be

$$\left\langle \text{kinetic energy} \right\rangle_2 = \frac{\omega_2^2}{\omega^2} \frac{\varepsilon}{2} \langle E^2 \rangle, \quad \frac{\varepsilon}{2} \langle E^2 \rangle = \text{time average stored electric energy} \qquad (b)$$

while the time average kinetic energy of the moving stream is

$$\left\langle \text{kinetic energy} \right\rangle_1 = - \frac{\omega_1^2}{u_o^2 \left[I_m \beta \right]^2} \frac{\varepsilon}{2} \langle E^2 \rangle \qquad (c)$$

By virtue of the dispersion relationship (a) the sum of these quantities is zero. Furthermore, the power flow is zero and there is no time average energy transfer to either stream, i.e., $i \cdot E = 0$ for both streams. Electrons in the moving stream must give up energy to field, but this is computed from $\langle i\,(x - u_o t)\, E(x - u_o t) \rangle$ not $\langle i(t) \cdot E(t) \rangle$. This has not been evaluated as yet, but it is expected that it will give the decrease in kinetic energy indicated by (c).

---

[1] H. Heffner, unpublished Bell Telephone Lab. Memorandum.

[2] J. R. Pierce, "Possible Fluctuations in Electron Streams due to Ions", JAP 19 231 (1948).

[3] R. Q. Twiss "On Bailey's Theory of Amplified Circularly Polarized Waves in an Ionized Medium", Phys.Rev.84 448 (1951).

Project F - A Study of the M-Carcinotron

Staff: J. W. Sadin, L. M. Field

To further extend the study of the conflict between starting current theory and starting current measurements which has been described in the French literature on M-carcinotrons, we have been attempting to insert the concept of slipping stream amplification into the M-carcinotron starting current analysis described in our Quarterly Report No. 4.

During the course of the coming quarter we will be building a simple model, low-power M-carcinotron for the purpose of checking starting current measurements vs. theory, obtaining experience with the operation of such devices, and comparing its relative efficiency with that of the backward-wave oscillator. The current design calls for a S-band tube using a flattened bifilar helix as the propagating circuit.

Project G - Application of Ferrites to Slow-Wave Propagating Structures

Staff: J. W. Sedin, C. C. Johnson, L. M. Field

In the belief that the application of ferrites to slow-wave propagating structures can result in much more efficient operation and shorter tubes in forward-wave amplifiers and perhaps novel forms of backward-wave oscillators and other types of interaction devices, we have begun experiments with ferrites. Our particular interest is the use of the ferrite in a region of circularly polarized magnetic field from a propagating structure.

To produce a system with large attenuation in one direction and very small attenuation in the opposite direction, dc demagnetization effects due to the position of the ferrite boundaries along the direction of the polarizing field have occupied our attention. It has been possible, for example, by proper attention to these effects, to vary the polarizing H-field necessary for the production of a large difference of attenuation in the two directions. From 4000 gauss to as low as 400 gauss at a checked frequency--for example, 9000 mc--using a given ferrite such as Ferramic J, some of these principles of guiding magnetic field along a ferrite and distorting the magnetic field direction into the proper direction for interaction with the circularly polarized H-field of the electromagnetic wave were strongly brought to our

attention by the important advances made at the Bell Telephone Laboratories using helical forms of ferrite which were described at the June 1954 Tube Conference at Orono, Maine. This use of the saturation flux density of a ferrite and of its properties as a fairly high permeability dc magnetic circuit in addition to its rf properties leads to interesting possibilities in the construction of ferrite unidirectional attenuators in traveling-wave tubes using a variety of possible slow-wave propagating structures.

We are continuing exploration of these possibilities.

PERSONNEL

L. M. Field	Project Head
R. W. Gould	3d Year Grad. Student - Physics
W. Buchman	3d Year Grad. Student - E. E.
J. W. Sedin	2d Year Grad. Student - E. E.
T. E. Feuchtwang	2d Year Grad. Student - E. E.
C. C. Johnson	1st Yr. Grad. Student - E. E.
E. V. Nogle	1st Yr. Grad. Student - E. E.

Professional Help

A. F. Carpenter	Glass Blower and Vacuum Tube Technician
Arthur Brown	Machinist

CALIFORNIA INSTITUTE OF TECHNOLOGY

DISTRIBUTION LIST

STATUS REPORTS (Nonr 220(13)

Addressee	Attn.	No. of Copies
Chief of Naval Research Navy Department Washington 25, D. C.	Code 427	7
Director Naval Electronics Laboratory San Diego 52, California		1
Commanding Officer Office of Naval Research Branch Office 1030 E. Green Street Pasadena, California		2
Chief, Bureau of Aeronautics Navy Department Washington 25, D. C.	EL 4	1
Chief, Bureau of Ordnance Navy Department Washington 25, D. C.	Re 4 Re 9	1 1
Committee on Electronics Research and Development Board Department of Defense Washington 25, D. C.		1
Microwave Laboratory Stanford University Stanford, California	F.V.L.Pindar	1
Massachusetts Institute of Technology Cambridge 39, Massachusetts	Research Laboratory of Electronics	1
Department of Electrical Engineering Yale University New Haven, Connecticut	H. J. Reich	1
Electrical Engineering Department University of Illinois Champaign, Illinois	Electron Tube Section	1
Electrical Engineering Department University of California Berkeley 4, California	Prof. T.C.McFarland Chairman	1

Cruft Laboratory Harvard University Cambridge, Massachusetts	E. L. Chaffee	1
Lincoln Laboratory Massachusetts Institute of Technology Cambridge 39, Massachusetts		1
Director, Electronics Defense Group Engineering Research Institute University of Michigan Ann Arbor, Michigan		1
Varian Associates 611 Hanson Way Palo Alto, California	Fred D. Wilimek	1
Bell Telephone Laboratories Murray Hill Laboratory Murray Hill, New Jersey	Leah E. Smith, Librarian	1
Hughes Aircraft Company Culver City, California	Mr. John T. Milek Technical Librarian	1
RCA Laboratories Princeton, New Jersey	Mr. E. W. Herold and Harwell Johnson	1
Federal Tele. Laboratories, Inc. 500 Washington Avenue Nutley, New Jersey	K. Wing	1
Columbia Radiation Laboratory 538 W. 120th Street New York 27, New York		1
Countermeasures Laboratory Gilfillan Bros., Inc. 1815 Venice Boulevard Los Angeles, California		1
The Motorola Corporation 4545 W. Augusta Boulevard Chicago, Illinois	John Byrne	1
Chief, Bureau of Aeronautics Department of the Navy Washington, D. C.	EL 43 EL 45	1 1
Chief, Bureau of Ships Department of the Navy Washington, D. C.	Code 816 820 840	1 1 1

Panel on Electron Tubes 346 Broadway (8th Floor) New York 13, New York		1
Librarian Electronics Research Laboratory Stanford University Stanford, California		1
Sperry Gyroscope Company Great Neck, Long Island New York	J. E. Shepherd	1
Raytheon Corporation Waltham, Massachusetts	H. R. Argento	1
Electron Tube Division of the Research Laboratory General Electric Company The Knolls Schenectady, New York	E. D. McArthur	1

UNCLASSIFIED